Journal of Computational Physics 229 (2010) 7765–7773

Contents lists available at ScienceDirect

Journal of Computational Physics

journal homepage: www.elsevier.com/locate/jcp

# An analytical-based method for studying the nonlinear evolution of localized vortices in planar homogenous shear flows

J. Cohen [a,*], I.G. Shukhman [b], M. Karp [a], J. Philip [a,1]

[a] Faculty of Aerospace Engineering, Technion – Israel Institute of Technology, Haifa 32000, Israel
[b] Institute of Solar–Terrestrial Physics, Russian Academy of Sciences, Siberian Department, P.O. Box 291, Irkutsk 664033, Russia

ARTICLE INFO

*Article history:*
Received 8 November 2009
Received in revised form 11 May 2010
Accepted 17 June 2010
Available online 25 June 2010

*Keywords:*
Localized vortex
Localized disturbance
Homogenous shear
Lagrangian coordinates

ABSTRACT

Recent experimental and numerical studies have shown that the interaction between a localized vortical disturbance and the shear of an external base flow can lead to the formation of counter-rotating vortex pairs and hairpin vortices that are frequently observed in wall bounded and free turbulent shear flows as well as in subcritical shear flows. In this paper an analytical-based solution method is developed. The method is capable of following (numerically) the evolution of finite-amplitude localized vortical disturbances embedded in shear flows. Due to their localization in space, the surrounding base flow is assumed to have homogeneous shear to leading order. The method can solve in a novel way the interaction between a general family of unbounded planar homogeneous shear flows and any localized disturbance. The solution is carried out using Lagrangian variables in Fourier space which is convenient and enables fast computations. The potential of the method is demonstrated by following the evolved structures of large amplitude disturbances in three canonical base flows, including simple shear, plane stagnation (extensional) and pure rotation flows, and a general case. The results obtained by the current method for plane stagnation and simple shear flows are compared with the published results. The proposed method could be extended to other flows (e.g. geophysical and rotating flows) and to include periodic disturbances as well.



## 1. Introduction

During the last 50 years it has become clear that although wall bounded turbulent shear flows are characterized by unsteady, seemingly chaotic motion, in fact, however, the motion is not random and it has been observed to be governed by well organized coherent vortical structures. In particular, the observation of counter-rotating streamwise vortices (CVP's), which lead to the formation of low and high-speed velocity regions (streaks), observed in the near wall region, and hairpin-shaped vortices extending across the boundary layer. Since their first experimental identification by Kline et al. [1], these coherent structures have come under intense investigations regarding their characterization, generation and sustenance mechanisms (e.g. [2,3]). The presence of streaky structures and their further breakup and appearance of hairpin vortices has been also observed in transitional flows (e.g. in laminar boundary layers [4]; subcritical channel flow [5]; pipe flow [6]). In free shear layers pairs of counter-rotating quasi-streamwise rib vortices are formed in the braid region, connecting the bottom part of the upstream spanwise Kelvin–Helmholtz roller with the top part of the downstream one (e.g. [7]).

* Corresponding author.
*E-mail address:* aerycyc@aerodyne.technion.ac.il (J. Cohen).
[1] Present address: Laboratoire d'Hydrodynamique (LadHyX), École Polytechnique, 91128 Palaiseau, France.

0021-9991/$ - see front matter © 2010 Elsevier Inc. All rights reserved.
doi:10.1016/j.jcp.2010.06.035

The similarity of the coherent structures naturally occurring in different fully developed boundary turbulent shear flows as well as in transitional flows and free shear layers suggests the existence of a basic mechanism responsible for the formation of these structures, under various base flow conditions. The common elements for all such flows are the *shear of the base flow* and the presence of a *localized vortical disturbance*. Recently, combining experimental, numerical and theoretical efforts, it was demonstrated [8–12] that a simple model, which takes into account only the interaction between a localized vortical disturbance and a laminar shear base flow, is capable of reproducing the generation process and characteristics of the coherent structures. This is schematically shown in Fig. 1. The interaction of a localized vortical disturbance (the orange vortex shown in the center of the figure) with pure shear flow (shown in the top left corner) results in the generation of a pair of streamwise vortices, in case the magnitude of the initial vortex is small and in the formation of a hairpin vortex when the initial magnitude is sufficiently high. This was shown numerically by Suponitsky et al. [11] (the two pictures in the top right corner). A similar process was experimentally obtained by Svizher and Cohen [5] when a disturbance was placed in Plane Poiseuille flow. The hairpin vortex shown in the middle right part was obtained by holographic particle image velocimetry (HPIV). Moreover, this simple interaction between a localized vortex and pure shear results in other characteristics such as the spanwise separation between the two elongated vortical regions of the CVP (expressed in terms of wall units), the inclination angle of the hairpins and their convective velocity, which correspond well to those observed in turbulent wall bounded shear flows. Similarly when a vortex dipole is placed in stagnation flow, CVP is developed along the principal axes of shear of the extensional flow [12] (bottom right corner). An example of such stagnation flow is the braid region of a turbulent mixing layer (shown by the red arrows in the bottom left picture) resulting from the superposition of the shear of the mixing layer and the Kelvin–Helmholtz spanwise instability 'rollers'.

The above brief summary demonstrates the possible significant role of localized disturbances in the evolution of several key coherent structures in various turbulent and transitional shear flows. By localized vortical disturbance it is meant that all the disturbance dimensions are much smaller than the characteristic length scale of the base flow. Accordingly, relative to the localized disturbance, the surrounding field may be considered as 'simple' laminar shear flow where the velocity components are (at most) linear functions of the coordinates. Thus, the main objective of the present work is to develop an accurate and efficient analytical-based method which can predict the nonlinear evolution of a localized dipole vortex in unbounded homogeneous shear flows. The proposed method solves efficiently (in Lagrangian space) the full Navier–Stokes equations by splitting it into 'base' ($\boldsymbol{V}$) and 'disturbance' ($\boldsymbol{v}$) equations (details of which are given below). The nonlinear equations corresponding to the disturbance are solved by considering a constant base flow strain matrix ($\partial \boldsymbol{V}/\partial \boldsymbol{x}$).

The use of *linear* equations to describe the evolution of a small disturbance embedded in base flow with constant strain matrix has been proved to be extremely useful to study the effect of rapid distortion on turbulence caused by the underlying shear flows. Analytical progress is assured in such cases due to the linearity of the governing equations. An excellent review of this subject and the 'problems' of turbulence is carried out by [13]. The present method begins with the usual Fourier transform of the equations, however with time-dependent wave numbers. The use of time-dependent wave number is certainly not novel and has been applied for stability problems in constant-shear flows beginning from the pioneering paper by Kelvin [14] (see also, for example, [15–17]). In the present paper an attempt is made to apply this approach in order to follow the nonlinear evolution of *localized disturbances*. The method is made efficient by solving the problem in a Fourier–Lagrangian space. Even though the price paid for passing onto Lagrangian space is a slight increase in complexity of the problem formulation, it is overshadowed by the efficiency and the ease of use, which the method provides (as demonstrated below).

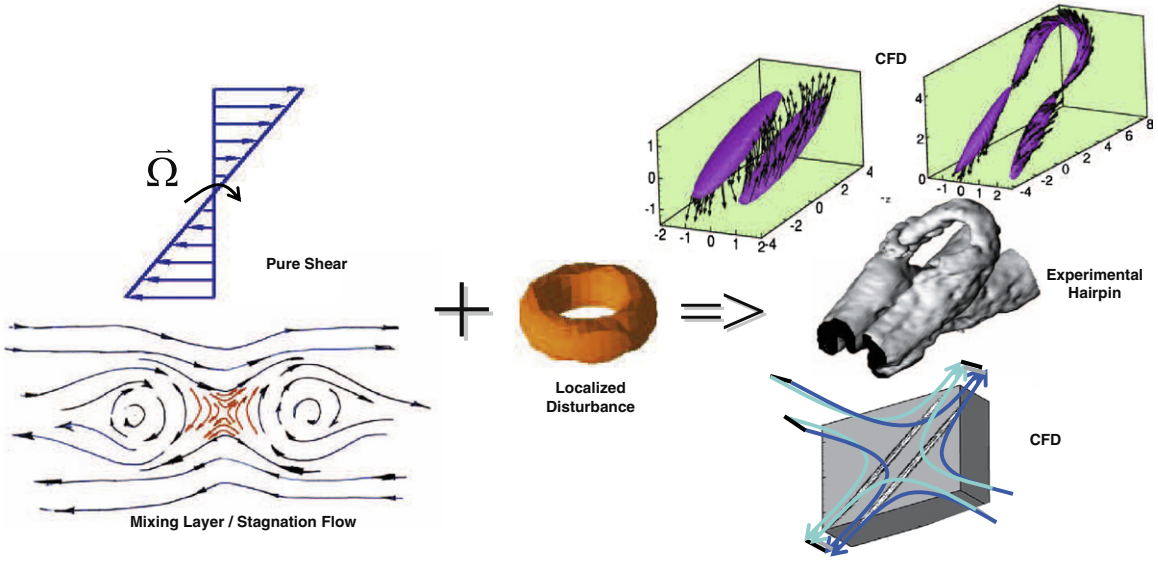


**Fig. 1.** Effect of interaction between shear flow and a localized disturbance. The numerical and experimental results are taken from [8].

The following proposed method can solve the interaction between any general base flow with constant strain matrix and a finite-amplitude localized disturbance. The capability of the method is demonstrated by following the evolved structures of large amplitude disturbances in three canonical base flows, namely simple shear, plane stagnation (extensional) and pure rotation flows. In addition, one example of a more general case is provided. The results concerning the nonlinear development of initially strong vortices for plane stagnation and Couette flows are compared and contrasted with previously published results using direct numerical simulation (DNS). It should be noted that the method could be easily extended to geophysical flows in order to follow the nonlinear evolution of thermals in unbounded environment with or without uniform stratification of density (or temperature) and with constant shear. It could also be extended to rotating flows, e.g. the investigation of the nonlinear evolution of a disturbance in Taylor–Couette flow (i.e. between two rotating cylinders) which for strongly localized disturbances may be considered as constant-shear flow with the presence of Coriolis force. Such an experiment is described in [18], while the linear stage of vortex evolution was followed (analytically) by this method in [19]. Besides following the nonlinear evolution of a localized disturbance, the method can be utilized to study the nonlinear evolution of periodic disturbances in flows with homogenous shear. Furthermore, combination of the two types of initial disturbances (localized and periodic) enables one to study several key transition scenarios (e.g. the use of the method to follow secondary instabilities and to understand the generation of packets of hairpins).

## 2. Mathematical–numerical approach

### 2.1. Problem formulation

We consider the evolution of a localized vortical disturbance. Accordingly, the initial disturbed vorticity is assumed to be confined to a small region in the flow field. Since the advection of the small disturbed region as a whole is not of interest, we use a Galilean frame, moving with the disturbance, instead of the laboratory frame. Consequently, the origin of the coordinate system is defined to be some point within the initially disturbed region at which the base flow velocity is stationary ($\boldsymbol{V}(0)=0$). A right handed cartesian coordinate system $\boldsymbol{x}=(x,y,z)$ is used with $\boldsymbol{V}=(U+u,V+v,W+w)$ being the corresponding velocity components. Capital and small letters designate, respectively, the base and disturbance velocity components. Taking advantage of the smallness of the disturbed region, it is assumed that a typical dimension of which ($\delta$) is much smaller than a dimensional length scale $\Delta$ corresponding to an $\mathcal{O}(1)$ change of the external velocity. Accordingly, the base velocity and vorticity fields around the origin are approximated by Taylor series expansions. Using the magnitude of the background shear (or vorticity) $|\boldsymbol{\Omega}|$ and the length scale $\Delta$ as the appropriate scales representing the external base flow, the Taylor series expansions are given by

$$V_m(\boldsymbol{x})=\frac{\partial V_m(0)}{\partial x_n}x_n\cdot\left[1+\mathcal{O}\left(\frac{|\boldsymbol{x}|}{\Delta}\right)\right],\quad \boldsymbol{\Omega}_m(\boldsymbol{x})=\boldsymbol{\Omega}_m(0)\cdot\left[1+\mathcal{O}\left(\frac{|\boldsymbol{x}|}{\Delta}\right)\right], \tag{1}$$

where $|\boldsymbol{x}|/\Delta\ll 1$, $m=1,2,3$ and repeating indices imply the usual summation convention (here, for $n=1,2,3$). Thus, with respect to finite-amplitude localized disturbances, the base flow velocity can be represented to leading order by its gradient tensor.

Without loss of generality the velocity and vorticity vectors for the planar case are respectively given by

$$\boldsymbol{V}=\left(-\frac{1}{2}(\Omega+\sigma)y,-\frac{1}{2}(\sigma-\Omega)x,0\right),\quad \boldsymbol{\Omega}=(0,0,\Omega), \tag{2}$$

where $\sigma$ and $\Omega$ are two constants representing the shear and vorticity of the base flow. The base flow is respectively hyperbolic (Fig. 2a), elliptic (Fig. 2b) or pure shear (Couette flow, Fig. 2c) for $|\sigma|>|\Omega|$, $|\sigma|<|\Omega|$ or $|\sigma|=|\Omega|$.

The equation describing the evolution of vorticity ($\boldsymbol{\omega}$) associated with a 3D finite-amplitude localized disturbance in incompressible viscous base flow is

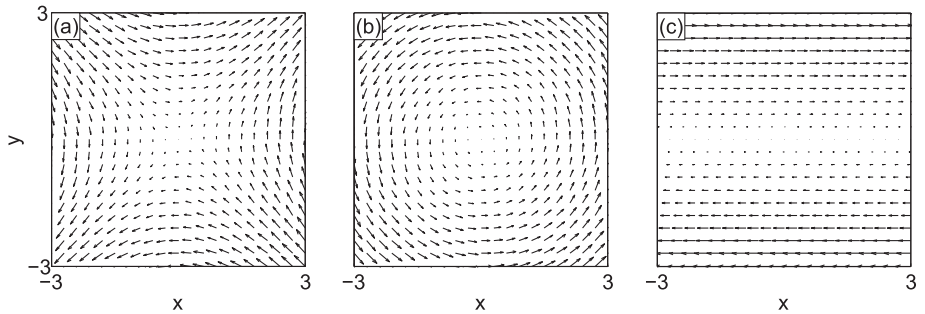


**Fig. 2.** Base flow examples: (a) hyperbolic (plane stagnation $\Omega=0$, $\sigma(=-80[1/s])<0$); (b) elliptic (pure rotation $\sigma=0$, $\Omega(=40[1/s])>0$) and (c) simple shear ($\Omega=\sigma(=-40[1/s])<0$).

$$\frac{\partial \boldsymbol{\omega}}{\partial t} + (\boldsymbol{V}\cdot\nabla)\boldsymbol{\omega} - (\boldsymbol{\omega}\cdot\nabla)\boldsymbol{V} - (\boldsymbol{\Omega}\cdot\nabla)\boldsymbol{v} = \nu\Delta\boldsymbol{\omega} + (\boldsymbol{\omega}\cdot\nabla)\boldsymbol{v} - (\boldsymbol{v}\cdot\nabla)\boldsymbol{\omega}, \tag{3}$$

where $t$ is time, $\nu$ the kinematic viscosity and the disturbance vorticity $\boldsymbol{\omega}$ and velocity $\boldsymbol{v}$ are related by $\boldsymbol{\omega} = \nabla \times \boldsymbol{v}$.

In what follows it is convenient to interchangeably associate the cartesian coordinates $x$, $y$ and $z$ with the subscripts 1, 2 and 3, respectively. Substituting (2) into (3), the three equations for the three disturbance vorticity components are

$$\mathcal{L}\omega_1 - \frac{1}{2}(\Omega-\sigma)\omega_2 - \Omega\frac{\partial v_3}{\partial x_1} = \nu\Delta\omega_1 + N_1, \tag{4a}$$

$$\mathcal{L}\omega_2 + \frac{1}{2}(\Omega+\sigma)\omega_1 - \Omega\frac{\partial v_3}{\partial x_2} = \nu\Delta\omega_2 + N_2, \tag{4b}$$

$$\mathcal{L}\omega_3 - \Omega\frac{\partial v_3}{\partial x_3} = \nu\Delta\omega_3 + N_3, \tag{4c}$$

where $\mathcal{L}$ is the convective operator:

$$\mathcal{L} = \frac{\partial}{\partial t} + V_1\frac{\partial}{\partial x_1} + V_2\frac{\partial}{\partial x_2} = \frac{\partial}{\partial t} - \frac{1}{2}(\sigma+\Omega)x_2\frac{\partial}{\partial x_1} - \frac{1}{2}(\sigma-\Omega)x_1\frac{\partial}{\partial x_2}, \tag{5}$$

and $N_m$, $m = 1,2,3$ represent the corresponding nonlinear terms, i.e.

$$N_m = \omega_n\frac{\partial v_m}{\partial x_n} - v_n\frac{\partial \omega_m}{\partial x_n}, \tag{6}$$

for which the summation convention is applied. It should be noted that (4c) could be alternatively replaced by the divergence free condition, i.e.

$$\frac{\partial \omega_1}{\partial x_1} + \frac{\partial \omega_2}{\partial x_2} + \frac{\partial \omega_3}{\partial x_3} = 0. \tag{7}$$

### 2.2. Transformation into Fourier space

The set of Eq. (4) are first Fourier transformed via

$$\hat{f}_m(\boldsymbol{k}) = \frac{1}{(2\pi)^3}\int f_m(\boldsymbol{r})\exp(-i\boldsymbol{k}\boldsymbol{r})d^3x, \quad f_m(\boldsymbol{r}) = \int \hat{f}_m(\boldsymbol{k})\exp(i\boldsymbol{k}\boldsymbol{r})d^3k, \tag{8}$$

where $m = 1,2,3$, $\hat{f}_m(\boldsymbol{k})$ being the Fourier transform and $f_m(\boldsymbol{r})$ its inverse transform, $\boldsymbol{r} = (x,y,z)$ is the real space physical vector and $\boldsymbol{k}$ its corresponding wave number vector in Fourier space.

The resulted set of equations is:

$$\mathcal{L}_k\hat{\omega}_1(\boldsymbol{k}) - \frac{1}{2}(\Omega-\sigma)\hat{\omega}_2(\boldsymbol{k}) - ik_1\Omega\hat{v}_3(\boldsymbol{k}) = -\nu k^2\hat{\omega}_1(\boldsymbol{k}) + \widehat{N}_1(\boldsymbol{k}), \tag{9a}$$

$$\mathcal{L}_k\hat{\omega}_2(\boldsymbol{k}) + \frac{1}{2}(\Omega+\sigma)\hat{\omega}_1(\boldsymbol{k}) - ik_2\Omega\hat{v}_3(\boldsymbol{k}) = -\nu k^2\hat{\omega}_2(\boldsymbol{k}) + \widehat{N}_2(\boldsymbol{k}), \tag{9b}$$

$$\mathcal{L}_k\hat{\omega}_3(bk) - ik_3\Omega\hat{v}_3(\boldsymbol{k}) = -\nu k^2\hat{\omega}_3(\boldsymbol{k}) + \widehat{N}_3(\boldsymbol{k}), \tag{9c}$$

where $k^2 = k_1^2 + k_2^2 + k_3^2$ and the operator $\mathcal{L}_k$ is given by

$$\mathcal{L}_k = \frac{\partial}{\partial t} + \frac{1}{2}(\sigma+\Omega)k_1\frac{\partial}{\partial k_2} + \frac{1}{2}(\sigma-\Omega)k_2\frac{\partial}{\partial k_1}. \tag{10}$$

The Fourier transform of each one of the products included in $N_m$ (see (6)) is the convolution of the corresponding Fourier transforms. Thus the expression for $\widehat{N}_m(\boldsymbol{k})$ can be written as:

$$\widehat{N}_m(\boldsymbol{k}) = i\int d^3k'\{k_n[v_m(\boldsymbol{k}')\omega_n(\boldsymbol{k}-\boldsymbol{k}') - v_n(\boldsymbol{k}')\omega_m(\boldsymbol{k}-\boldsymbol{k}')]\}. \tag{11}$$

### 2.3. Transition into Lagrangian variables in $\boldsymbol{k}$-space

Following [9] the resulted set of Eq. (9) is expressed in terms of Lagrangian coordinates in the Fourier space. For this, we demand that the operator $\mathcal{L}_k$ be the substantial derivative along an unperturbed trajectory in $\boldsymbol{k}$-space, i.e.

$$\mathcal{L}_k = \frac{\partial}{\partial t} + \frac{1}{2}(\sigma+\Omega)k_1\frac{\partial}{\partial k_2} + \frac{1}{2}(\sigma-\Omega)k_2\frac{\partial}{\partial k_1} \equiv \frac{d}{dt} = \frac{\partial}{\partial t} + \frac{dk_1}{dt}\frac{\partial}{\partial k_1} + \frac{dk_2}{dt}\frac{\partial}{\partial k_2} + \frac{dk_3}{dt}\frac{\partial}{\partial k_3}. \tag{12}$$

This leads to the following set of equations describing the temporal evolution of the wave vector $\boldsymbol{k}$:

$$\frac{dk_1}{dt} = \frac{1}{2}(\sigma - \Omega)k_2, \quad \frac{dk_2}{dt} = \frac{1}{2}(\Omega + \sigma)k_1, \quad \frac{dk_3}{dt} = 0, \tag{13}$$

the solution of which is:

$$\boldsymbol{k} = \hat{\mathcal{M}}\boldsymbol{q}, \quad \hat{\mathcal{M}} = \begin{pmatrix} \cosh\kappa t & \lambda^{1/2}\sinh\kappa t & 0 \\ \lambda^{-1/2}\sinh\kappa t & \cosh\kappa t & 0 \\ 0 & 0 & 1 \end{pmatrix} \quad \text{for } \lambda \neq 0, \tag{14}$$

where the initial value of $\boldsymbol{k}(t=0) = \boldsymbol{q}$ and the base flow parameters $\kappa$ and $\lambda$ are respectively defined as:

$$\kappa = \frac{1}{2}\sqrt{\sigma^2 - \Omega^2}\cdot \mathrm{sign}(\sigma), \quad \lambda = \frac{\sigma - \Omega}{\sigma + \Omega}. \tag{15}$$

It is noted that the matrix $[\widehat{\mathcal{M}}(t)]^T$ is closely related to the transformation matrix used by Rogallo [15], which appears when the transformation to Lagrangian variables is made in real space rather than in Fourier space. For $|\sigma| < |\Omega|$ the parameter $\kappa$ is pure imaginary and the flow is elliptic. For $\sigma = 0$, the expression sign ($\sigma$) in (15) is replaced by sign ($\Omega$) and the flow is pure rotational. Positive and negative values of $\lambda$ respectively correspond to hyperbolic and elliptic base flows, whereas the particular cases $\lambda = 1, -1$ and 0 are associated with pure extensional flow, pure rotational flow and parallel shear (unbounded Couette) flow, respectively. For the latter case, the matrix $\hat{\mathcal{M}}$ is given by

$$\widehat{\mathcal{M}} = \begin{pmatrix} 1 & 0 & 0 \\ \Omega t & 1 & 0 \\ 0 & 0 & 1 \end{pmatrix} \quad \text{for } \lambda = 0. \tag{16}$$

Designating,

$$\zeta(\boldsymbol{q}, t) = \hat{\omega}(\boldsymbol{k}(\boldsymbol{q}, t), t), \tag{17}$$

and utilizing the simple algebraic relation between the Fourier transformed velocity and vorticity vectors, i.e.

$$\hat{\boldsymbol{v}}(\boldsymbol{k}) = ik^{-2}[\boldsymbol{k} \times \hat{\boldsymbol{\omega}}(\boldsymbol{k})], \tag{18}$$

lead to the following final set of equations:

$$\frac{d\zeta_1(\boldsymbol{q}, t)}{dt} = -\frac{1}{2}(\sigma - \Omega)\zeta_2(\boldsymbol{q}, t) - \Omega k^{-2}k_1[k_1\zeta_2(\boldsymbol{q}, t) - k_2\zeta_1(\boldsymbol{q}, t)] - \nu k^2\zeta_1(\boldsymbol{q}, t) + \widehat{N}_1(\boldsymbol{q}, t), \tag{19a}$$

$$\frac{d\zeta_2(\boldsymbol{q}, t)}{dt} = -\frac{1}{2}(\sigma + \Omega)\zeta_1(\boldsymbol{q}, t) - \Omega k^{-2}k_2[k_1\zeta_2(\boldsymbol{q}, t) - k_2\zeta_1(\boldsymbol{q}, t)] - \nu k^2\zeta_2(\boldsymbol{q}, t) + \widehat{N}_2(\boldsymbol{q}, t), \tag{19b}$$

$$\frac{d\zeta_3(\boldsymbol{q}, t)}{dt} = \Omega k^{-2}k_3[k_1\zeta_2(\boldsymbol{q}, t) - k_2\zeta_1(\boldsymbol{q}, t)] - \nu k^2\zeta_3(\boldsymbol{q}, t) + \widehat{N}_3(\boldsymbol{q}, t), \tag{19c}$$

where (19c) could be alternatively replaced by

$$\zeta_3(\boldsymbol{q}, t) = -k_3^{-1}[k_1\zeta_1(\boldsymbol{q}, t) + k_2\zeta_2(\boldsymbol{q}, t)]. \tag{20}$$

### 2.4. Numerical procedure

The advantage of the theoretical model described above is that the nonlinear partial differential equations for the vorticity disturbance in the physical space are replaced by corresponding ordinary nonlinear equations. In the following a simple numerical procedure is outlined for solving these equations. We first choose the initial vortical disturbance in the physical space, transform it into Fourier space where we perform numerical integration of the Lagrangian variables, and finally, at a predetermined time, the spatial structure of the disturbance vorticity in the physical space is obtained by executing an inverse Fourier transform back to the physical space. For a given initial vortex the final solution is obtained (within minutes on a standard laptop) using the software, MATLAB. It is noted that, for a similar calculation, the time required to perform a DNS with the commercial software FLUENT is more than two orders of magnitude. Apart from the time, one has to write large amounts of additional programs for the insertion/extraction of initial disturbance and further post-processing. Such a procedure is completely absent in the current method. Moreover, in the present method, shifting to any linear base flow and to any kind of localized disturbance can easily be achieved. Some examples are presented in Section 3.

#### 2.4.1. Initial conditions and flow parameters

Although any divergence free vortex disturbance could be chosen, it is convenient to follow the temporal evolution of a localized Gaussian vortex for which the vorticity field and its Fourier transform are respectively given by

$$\boldsymbol{\omega}(r,t=0)=\nabla F\times P_0,\quad F=(\pi^{1/2}\delta)^{-3}\exp(-r^2/\delta^2), \tag{21}$$

$$\hat{\boldsymbol{\omega}}(k,t=0)=\zeta(q,t=0)=\frac{i}{(2\pi)^3}(q\times P_0)\exp\left(-\frac{1}{4}q^2\delta^2\right), \tag{22}$$

where $r$ is the spherical radial co-ordinate, $\delta$ is the representative length scale of the disturbance and $\boldsymbol{P}_0$ is its initial fluid impulse. The strength of the initial vortex is characterized by $\varepsilon=\omega_{\max}(t=0)/\Omega^*$, where $\omega_{\max}(t=0)=0.154|\boldsymbol{P}_0|/\delta^4$ for the Gaussian vortex, $\Omega^*=\frac{1}{2}(|\Omega|+|\sigma|)$ and $\omega_{\max}(t)=\max|\boldsymbol{\omega}(\boldsymbol{r},t)|$. The magnitude of $\varepsilon$ is used to describe an initial vortex as linear ($\varepsilon\ll 1$) or nonlinear. The effect of viscosity is represented by the 'vortex Reynolds number', $\mathrm{Re}=\Omega^*\delta^2/\nu$. In the following all length scales are normalized by $\delta$ and time scales by $1/\Omega^*$.

*2.4.2. Numerical integration*

After the initial vorticity field is transformed into the Fourier space, Eq. (19) is integrated in time using the Euler method. The evaluation of the convolution sums in the nonlinear terms on the right hand sides of (19) is carried out by utilizing a pseudospectral transform method (e.g. [20,21]). Accordingly, at a given time step, using (14), (18) and (16), each one of the two terms constituting the multiplication products in $\widehat{N}_m(k)$ $m=1,2,3$ (e.g. $v_n$ and $\partial\omega_m/\partial x_n$ in $v_n\partial\omega_m/\partial x_n$), is transformed back to the physical space via inverse FFT, where their multiplication is carried out. Similarly, all the multiplication products included in $\widehat{N}_m(k)$ are transformed into the physical space and the sum of which is transformed back to the Fourier space via FFT. Aliasing removal is done by truncation; however, for the results presented below where the disturbance dies out rapidly, there is no need for this procedure providing the physical domain is sufficiently large.

*2.4.3. Calculation of the vorticity components in the physical space*

The vorticity components $\omega_m$ in the physical space is given by

$$\omega_m(r,t)=\int d^3k\hat{\omega}_m(k,t)e^{i\mathbf{kr}}. \tag{23}$$

However, this is not a straight forward step because the wave number vector $\boldsymbol{k}$ depends on time. To avoid this difficulty the relation between the physical coordinates $\boldsymbol{r}_0=(x_0,y_0,z_0)$, indicating the coordinates of the initial position of a fluid particle at time $t=0$ and the coordinates $\boldsymbol{r}=(x,y,z)$ where the same particle has arrived at time $t$ (following an unperturbed trajectory), has to be derived. To do so we first pass from integration in $\boldsymbol{k}$ space to integration in $\boldsymbol{q}$, using the incompressibility condition, i.e. $d^3k=d^3q$, and the relation

$$k\cdot r=q\cdot r_0. \tag{24}$$

The above expression can be proven as follows:

$$k\cdot r=k_m x_m=\hat{\mathcal{M}}_{mn}q_n x_m=q_n(\hat{\mathcal{M}}^T_{nm}x_m)=q_n x_{0n}=q\cdot r_0, \tag{25}$$

where $\hat{\mathcal{M}}$ is the matrix relating $\boldsymbol{k}$ and $\boldsymbol{q}$ (14), the superscript $T$ indicates a transposed matrix and $x_{0n}$ are the initial physical coordinates of the fluid particle. Finally we obtain

$$\omega_m(r,t)=\omega_m(r_0(r,t))=\int d^3q\zeta_m(q,t)e^{i[q_1x_0(\mathbf{r},t)+q_2y_0(\mathbf{r},t)+q_3z_0]}, \tag{26}$$

where the relation between the initial position of the fluid particle and the position at time $t$, is given (using (25)) by $r_0=[\hat{\mathcal{M}}(t)]^T r$.

## 3. Results

The purpose of this section is to demonstrate the capabilities of the mathematical–numerical approach described above. Results for three canonical base flows, namely simple shear ($\lambda=0$), pure extensional flow ($\lambda=1$) and pure rotational flow ($\lambda=-1$) are presented, followed by a more general case for which $\lambda=-0.2$. Before presenting the nonlinear results it is important to note that the results associated with various linear cases were successfully compared with corresponding linear theory. In particular, with the linear solutions for elliptic flow [10], for pure extensional flows [22] and for arbitrary hyperbolic flows [9].

The results associated with the evolution of nonlinear vortices in pure extensional flow and simple shear (Couette) are compared with previously obtained DNS. For this purpose the values of $\delta=0.001[\mathrm{m}]$, $\nu=10^{-6}[\mathrm{m}^2/\mathrm{s}]$ (corresponding to water) and vortex Reynolds number $\mathrm{Re}=\Omega^*\delta^2/\nu=40$ are taken in the calculations presented here. For the case of pure rotation and for the more general case new results are presented for the same Reynolds number.

Fig. 3 shows the temporal evolution of the vortical structure embedded in plane stagnation flow (left column), simple shear (middle column) and pure rotation (right column). The structures are shown by plotting iso-surfaces of vorticity magnitude ($|\boldsymbol{\omega}|/\omega_{\max}=0.7$ for plane stagnation and pure rotation flows and $|\boldsymbol{\omega}|/\omega_{\max}=0.6$ for simple shear). In the plane stagnation flow ($\Omega=0$, $\sigma=-80[1/\mathrm{s}]$), the initial toroidal shape at $T\equiv\Omega^*t=0$ is developed into a counter-rotating vortex pair ($T=1$) which by $T=2$ is further extended along the $X=Y$ axis. As the initial magnitude of the vortex is relatively high

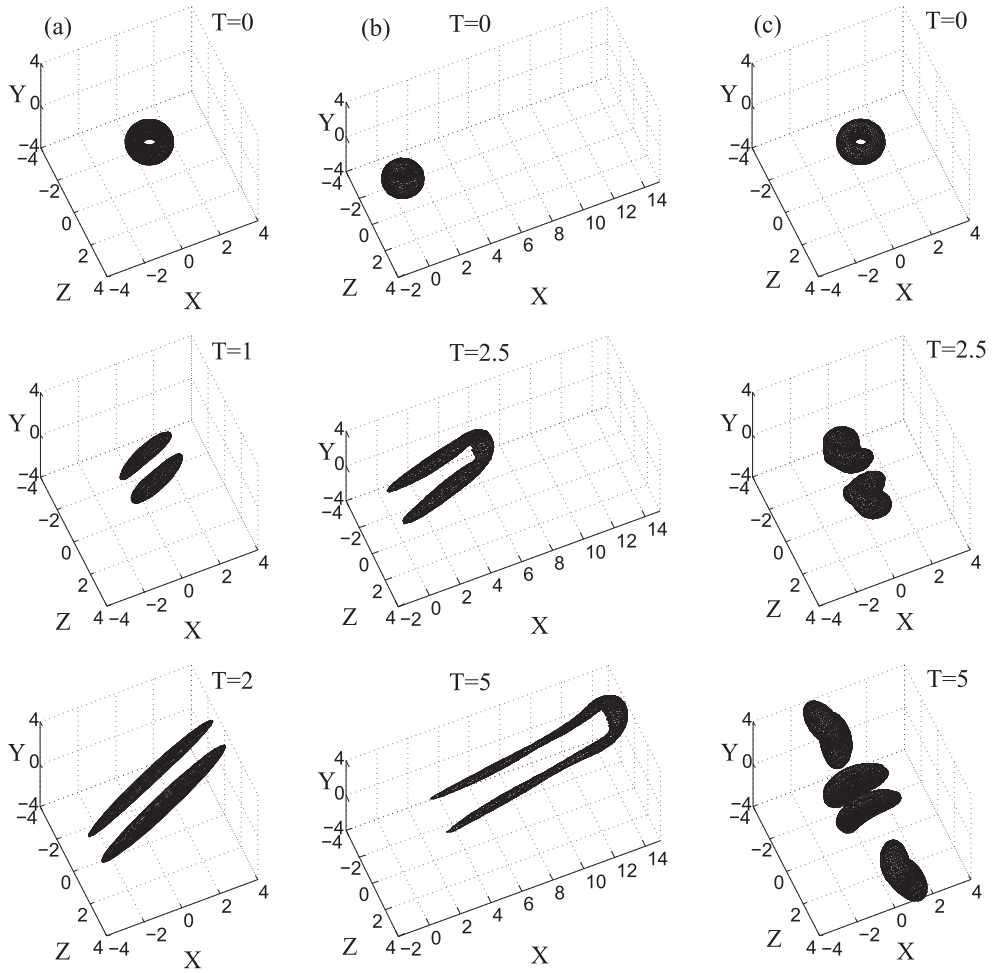


**Fig. 3.** Temporal evolution of localized vortices shown by vorticity iso-surfaces for (a) plane stagnation ($\varepsilon = 1$, $|\boldsymbol{\omega}|/\omega_{max} = 0.7$); (b) simple shear ($\varepsilon = 7.5$, $|\boldsymbol{\omega}|/\omega_{max} = 0.6$) and (c) pure rotation ($\varepsilon = 1$, $|\boldsymbol{\omega}|/\omega_{max} = 0.7$).

$\boldsymbol{P}_0 = (0, 2.5 \cdot 10^{-10}, 0)[m^4/s]$, ($\varepsilon = 1$), its center moves away from the origin due to self-induced motion [12]. When a strong initial vortex $\boldsymbol{P}_0 = (0, 1.95 \cdot 10^{-9}, 0)[m^4/s]$, ($\varepsilon = 7.5$) is initially placed in simple shear (plane Couette flow, $\Omega = \sigma = -40[1/s]$), the evolved structure (at $T = 4$) is that of a hairpin vortex. In the pure rotation base flow ($\Omega = 80[1/s]$, $\sigma = 0$), the nonlinear initial toroidal vortex ($\boldsymbol{P}_0 = (0, 2.5 \cdot 10^{-10}, 0)[m^4/s]$, $\varepsilon = 1$) rotates around the $z$ axis and splits into two symmetrical parts by $T = 2.5$ and splits again at $T = 5$. While $\omega_{max}$ increases with time for plane stagnation flow, it stays approximately the same for simple shear (although the associated enstrophy integral is growing [11]) and in pure rotation it decreases rapidly.

The distributions of the dimensional vorticity magnitude (corresponding to the results presented in Fig. 3) along three orthogonal axes at a fixed time ($T = 1$ for plane stagnation and pure rotation flows and $T = 5$ for simple shear), are indicated in Fig. 4 by the plus symbols connected with solid lines. The results for plane stagnation flow, simple shear and pure rotation are shown on the left (a), middle (b) and right (c) columns, respectively. For the plane stagnation flow and simple shear the distributions are compared with corresponding results (shown by the circles connected with dotted lines), previously obtained by Philip and Cohen [12] and Suponitsky et al. [11], respectively. For the pure rotation case we compare the results obtained by the Euler method (in time) with the results of a second order Runge–Kutta method. For plane stagnation flow the distributions are along the principal axes of the velocity gradient tensor $X = Y$, $Z = 0$ (axis of extension), $X = -Y$, $Z = 0$ (axis of compression) and $X = Y = 0$, $Z$. Nonlinearity is evident by the non-symmetrical distributions along the first two axes. Good agreement is obtained between the present calculations and the results obtained by DNS. For the strong nonlinear disturbance placed in simple shear the agreement at $T = 5$ is also very good. It should be noted that in the present calculations the vortical structure is embedded in unbounded simple shear whereas the numerical results obtained by Suponitsky et al. [11] are for Couette flow bounded between two walls. For the pure rotational flow the initial disturbance magnitude is identical to the one of the plane stagnation flow and it can be seen that by the time $T = 1$, the vorticity magnitude along $X$, $Y$ and $Z$ in this case is smaller than the one obtained in the plane stagnation. The results obtained by the two time integration methods are almost identical; slight deviations could be observed only at longer times (not shown here). As we also have not

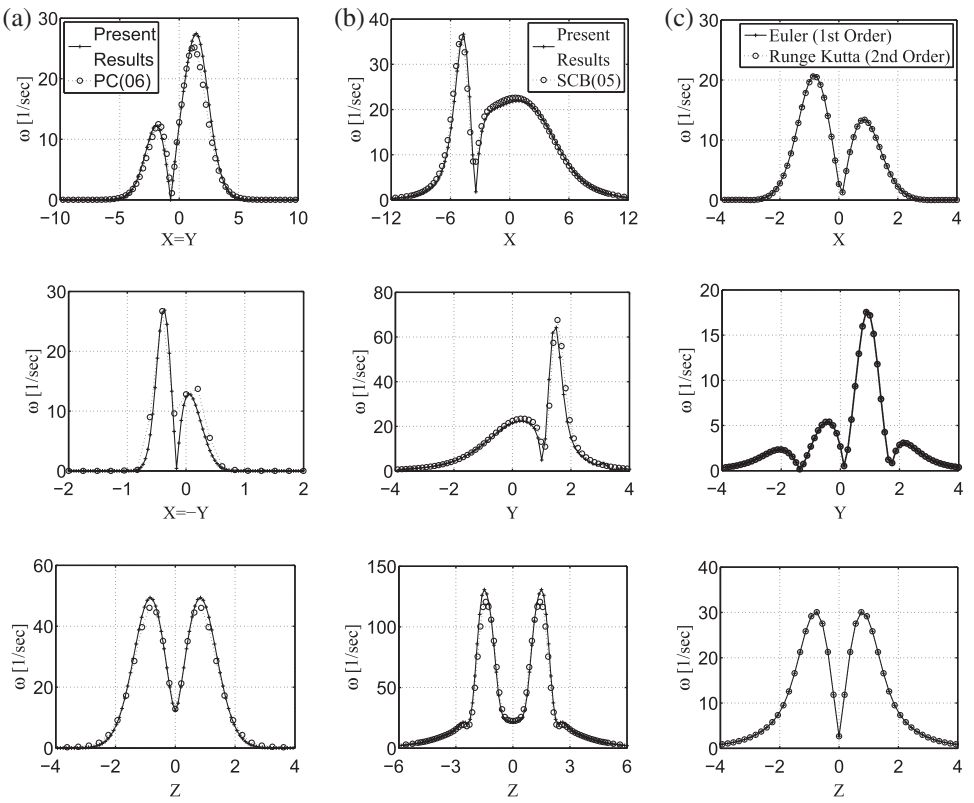


**Fig. 4.** Axial distributions of vorticity magnitudes corresponding to the results presented in Fig. 3 for (a) plane stagnation-comparison with PC (06) [12] ($\varepsilon = 1$, $T = 1$); (b) simple shear-comparison with SCB (05) [11] ($\varepsilon = 7.5$, $T = 5$); (c) pure rotation – comparison between Euler and second order Runge–Kutta integration methods in time ($\varepsilon = 1$, $T = 1$).

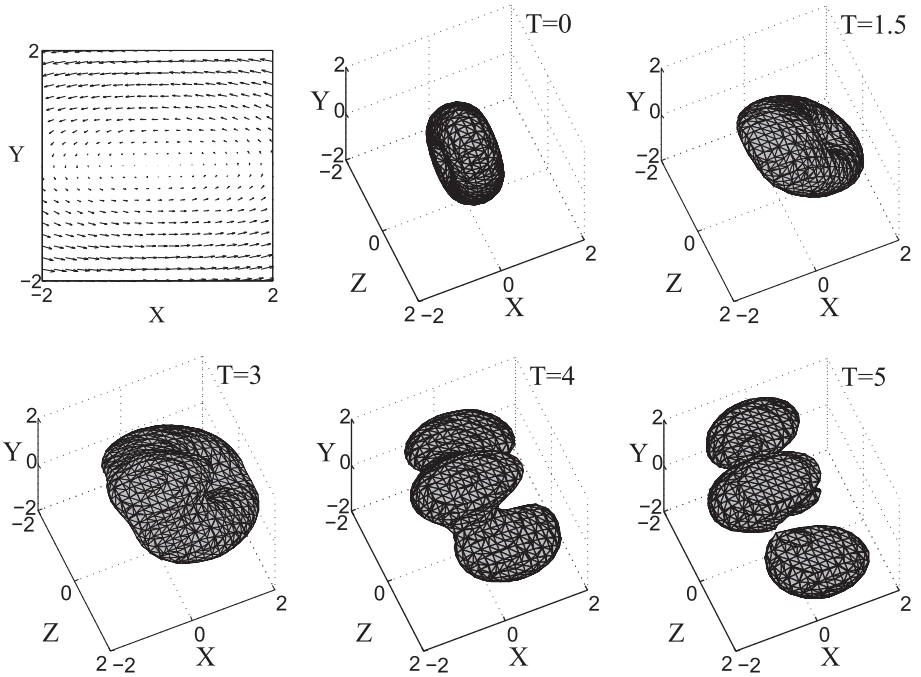


**Fig. 5.** The base flow (top left) and iso-surfaces of $|\boldsymbol{\omega}|/\omega_{\max} = 0.7$ at various times for a general case of elliptic base flow ($\sigma = 32$[1/s] and $\Omega = 48$[1/s]), $\varepsilon = 1$.

noticed any significant difference between the results obtained by the Euler and the second order Runge–Kutta methods for the rest of the results presented in this paper, we chose the use of the Euler method for its simplicity and efficiency. Nevertheless, it should be noted that any integration method could be implemented in our proposed algorithm.

Finally the evolved structures for the more general case for which $\sigma = 32[1/s]$ and $\Omega = 48[1/s]$ ($\Omega^* = 40$) are shown in Fig. 5 by plotting iso-surfaces of vorticity magnitude ($|\boldsymbol{\omega}|/\omega_{max} = 0.7$). On the top left corner of the figure the base flow velocity field is plotted. For this case the base flow is elliptical ($|\sigma| < |\omega|$) and therefore the streamlines are closed. Here we follow the evolution in time of a nonlinear Gaussian vortex for which the initial fluid impulse is aligned along the positive $x$-axis ($\boldsymbol{P}_0 = (2.5 \cdot 10^{-10}, 0, 0)[m^4/s]$, $\varepsilon = 1$). The structure first rotates ($T = 1.5$) and then by $T = 4$ begins to split into three major parts (an additional smaller part can be observed at $T = 5$ beneath the center part). In this case the enstrophy of the vortex decreases with time.

## 4. Conclusions

The evolution of localized vortical disturbances in homogenous shear can lead to the development of key structures (e.g. CVPs and hairpin vortices) that have been observed in turbulent and transitional shear flows. We have developed an efficient analytical-based method which allows to predict the nonlinear evolution of localized vortices in any planar homogenous shear flow. In this novel method, the solution is carried out using Lagrangian variables in Fourier space. Comparison to available results in the literature shows high fidelity of the current method. Finally, it is worth mentioning that the presented method can be extended without much effort to solve the transport of any nonlinear, localized, scalar quantity as well as periodic disturbances in homogeneous shear flows. Among others, the set of such equations includes buoyancy driven incompressible flow and transport of pollutants and chemical species.

## Acknowledgments

This research has been supported by the Israeli Science Foundation under Grant No. 1247/06. Ilia Shukhman would like to acknowledge the support by Russian Foundation for Basic Research, RFBR Grants Nos. 09-02-00082 and 10-05-00094, "Leading Scientific Schools" Grant No. 900.2008.2 provided by the Ministry of Industry, Science, and Technology of Russian Federation, and also by Programs of presidium of Russian Academy of Sciences No. 16 and OFN RAS No. 16.

## References

[1] S.J. Kline, W.C. Reynolds, F.A. Schraub, P.W. Runstadler, The structure of turbulent boundary layers, J. Fluid Mech. 30 (1967) 741–773.
[2] S.K. Robinson, Coherent motions in the turbulent boundary layers, Ann. Rev. Fluid Mech. 23 (1991) 601–639.
[3] R.L. Panton, Self-Sustaining Mechanisms of Wall Turbulence, Computational Mechanics Publications, Southampton, 1997.
[4] M.S. Acarlar, C.R. Smith, A study of hairpin vortices in a laminar boundary layer. Part 1: Hairpin vortices generated by a hemisphere protuberance, J. Fluid Mech. 175 (1987) 1–41.
[5] A. Svizher, J. Cohen, Holographic particle image velocimetry measurements of hairpin vortices in a subcritical air channel flow, Phys. Fluids 18 (2006) 014105.
[6] J. Cohen, J. Philip, G. Ben-Dov, Aspects of linear and nonlinear instabilities leading to transition in pipe and channel flows, Philos. Trans. Roy. Soc. A 367 (2009) 509527.
[7] L.P. Bernal, A. Roshko, Streamwise vortex structure in plane mixing layers, J. Fluid Mech. 170 (1986) 499–525.
[8] J. Cohen, V. Suponitsky, P.Z. Bar-Yoseph, A. Svizher, J. Philip, Localized disturbances and their relation to turbulent shear flows, in: AIAA-3226, Proceedings of the 36th AIAA Fluid Dynamics Conference and Exhibit, San Francisco, California, USA.
[9] I.G. Shukhman, Evolution of a localized vortex in plane nonparallel viscous flows with constant velocity shear. I: Hyperbolic flow, Phys. Fluids 18 (2006) 097101.
[10] I.G. Shukhman, Evolution of a localized vortex in plane nonparallel viscous flows with constant velocity shear. II: Elliptic flow, Phys. Fluids 19 (2007) 017106.
[11] V. Suponitsky, J. Cohen, P.Z. Bar-Yoseph, The generation of streaks and hairpin vortices from a localized vortex embedded in unbounded uniform shear flow, J. Fluid Mech. 535 (2005) 65–100.
[12] J. Philip, J. Cohen, The evolution of a finite-amplitude localized disturbance in an irrotational unbounded plane stagnation flow, J. Fluid Mech. 555 (2006) 459–473.
[13] J.C.R. Hunt, D.J. Carruthers, Rapid distortion theory and the problems of turbulence, J. Fluid Mech. 212 (1990) 497–532.
[14] Lord Kelvin (W. Thomson), Stability of fluid motion: rectilinear motion of viscous fluid between two parallel plates, Philos. Mag. 24 (5) (1887) 188–196.
[15] R.S. Rogallo, Numerical experiments in homogeneous turbulence, NASA Tech. Memo. 81315 (1981) 1–56.
[16] A.D.D. Craik, W.O. Criminale, Evolution of wavelike disturbances in shear flows: a class of exact solutions of the Navier–Stokes equations, Proc. Roy. Soc. Lond. A 406 (1986) 13–26.
[17] H. Hanazaki, J.C.R. Hunt, Structure of unsteady stably stratified turbulence with mean shear, J. Fluid Mech. 507 (2004) 1–42.
[18] E. Malkiel, V. Levinski, J. Cohen, The evolution of a localized vortex disturbance in external shear flows. Part 2: Comparison with experiments in rotating shear flows, J. Fluid Mech. 379 (1999) 351–380.
[19] I.G. Shukhman, V. Levinski, Temporal evolution of localized weak vortex in viscous circular shear flows, Phys. Fluids 17 (2005) 017104.
[20] S.A. Orszag, Numerical simulation of incompressible flows within simple boundaries. I: Galerkin (spectral) representations, Stud. Appl. Math. 50 (1971) 293–327.
[21] S.A. Orszag, Transform method for calculation of vector coupled sums: application to the spectral form of the vorticity equation, J. Atmos. Sci. 27 (1970) 890–895.
[22] A. Leonard, Turbulence structure and vortex dynamics, Cambridge University Press, 2000.